Protein Science (2000), *9*:1282–1293. Cambridge University Press. Printed in the USA.

NMR structure of a concatemer of the first and second ligand-binding modules of the human low-density lipoprotein receptor

NYOMAN D. KURNIAWAN,[1] ANNETTE R. ATKINS,[1] STEPHAN BIERI,[1] CATHERINE J. BROWN,[1] IAN M. BRERETON,[2] PAULUS A. KROON,[1] AND ROSS SMITH[1]

[1]Department of Biochemistry, University of Queensland, QLD 4072, Australia
[2]Centre for Magnetic Resonance, University of Queensland, QLD 4072, Australia

(RECEIVED February 11, 2000; ACCEPTED May 5, 2000)

Abstract

The ligand-binding domain of the human low-density lipoprotein receptor consists of seven modules, each of 40–45 residues. In the presence of calcium, these modules adopt a common polypeptide fold with three conserved disulfide bonds. A concatemer of the first and second modules ($LB_{1–2}$) folds efficiently in the presence of calcium ions, forming the same disulfide connectivities as in the isolated modules. The three-dimensional structure of $LB_{1–2}$ has now been solved using two-dimensional ^{1}H NMR spectroscopy and restrained molecular dynamics calculations. No intermodule nuclear Overhauser effects were observed, indicating the absence of persistent interaction between them. The near random-coil NH and Hα chemical shifts and the low ϕ and ψ angle order parameters of the four-residue linker suggest that it has considerable flexibility. The family of $LB_{1–2}$ structures superimposed well over LB_1 or LB_2, but not over both modules simultaneously. LB_1 and LB_2 have a similar pattern of calcium ligands, but the orientations of the indole rings of the tryptophan residues W23 and W66 differ, with the latter limiting solvent access to the calcium ion. From these studies, it appears that although most of the modules in the ligand-binding region of the receptor are joined by short segments, these linkers may impart considerable flexibility on this region.

Keywords: concatemer; LDL receptor; ligand-binding domain; NMR spectroscopy; protein structure

The low-density lipoprotein receptor (LDLR) plays a pivotal role in the removal of cholesterol-rich lipoproteins from the circulation (Havel & Kane, 1995). LDLR binds to its ligands, apolipoprotein (apo) B-100 and apoE, of LDL and intermediate-density lipoproteins, promoting their uptake by receptor-mediated endocytosis. Upon uptake, the receptor-ligand complex transits in endosomes, where the receptor separates from its ligand, and recycles back to the cell surface (Goldstein et al., 1985; Brown & Goldstein, 1986; Johnson et al., 1997).

The LDLR consists of ligand binding (LB), epidermal growth factor (EGF) precursor homology, O-linked sugar, transmembrane, and cytoplasmic domains. The arrangement of these domains is similar to that of other members of the LDLR gene family, including the VLDL receptor (Takahashi et al., 1992), the LDL receptor-related protein (LRP) (Herz et al., 1988), and the renal glycoprotein gp330/megalin (Saito et al., 1994). The ligand-binding domain consists of seven imperfect repeats, each of 40–45 residues. The three-dimensional (3D) structures of the two N-terminal repeats, LB_1 and LB_2, have been solved by NMR spectroscopy (Daly et al., 1995a, 1995b), and LB_5 by X-ray crystallography (Fass et al., 1997). Approximately 40% of the residues are conserved across the seven modules, including all cysteine residues, an isoleucine, and the D-x-S-D-E motif (Fig. 1). The cysteine residues, which have a conserved I–III, II–V, and IV–VI pattern (Bieri et al., 1995a, 1995b, 1998), stabilize the backbone fold of the LB modules. In the modules of known structure, the isoleucine residues are located within a small hydrophobic core; and in LB_5, the last two residues of the D-x-S-D-E motif are involved in calcium binding.

Reprint requests to: Ross Smith, Department of Biochemistry, University of Queensland, QLD 4072, Australia; e-mail: ross@biosci.uq.edu.au.

Abbreviations: DQF-COSY, double-quantum filtered correlated spectroscopy; DYANA, dynamics algorithm for NMR applications; E-COSY, exclusive correlated spectroscopy; LDL, low-density lipoprotein; LRP, LDL receptor-related protein; LB_1 to LB_7, cysteine-rich modules number 1 to 7 of the ligand-binding domain of LDL receptor; $LB_{1–2}$ and $LB_{5–6}$, concatemers of the first and second, and fifth and sixth, ligand-binding modules of the LDL receptor; CR_3 and CR_8, complement-like repeats number 3 and 8 of LRP; VLDL, very low-density lipoprotein; NOE, nuclear Overhauser effect; NOESY, nuclear Overhauser effect spectroscopy; PBS, phosphate-buffered saline; RMSD, root-mean-square deviation; RP-HPLC, reversed-phase high-performance liquid chromatography; TOCSY, total correlation spectroscopy.

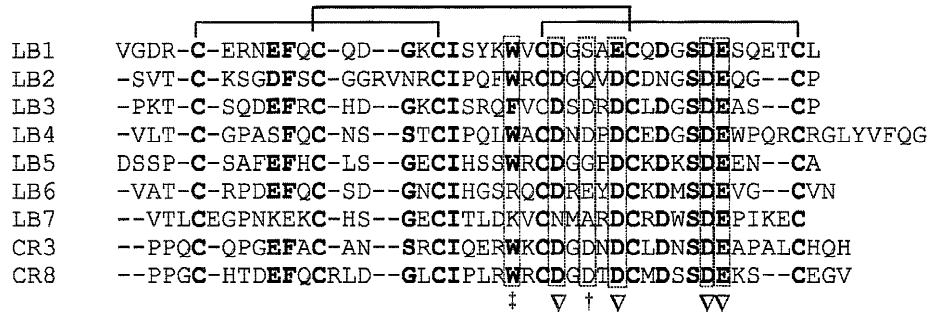

Fig. 1. Amino acid sequences of the ligand binding modules (LB) of the LDL receptor and two of the complement-like repeats (CR) of the LDL receptor-related protein. The disulfide bond connectivities (I–III, II–V, and IV–VI) are shown above the sequences. The conserved amino acids are shown in bold, and the amino acids for which carboxyl (▽) or carbonyl (‡,†) groups may be involved in calcium coordination are shown in brackets.

Recent studies with LB_1 and LB_2 have shown that calcium ions are required for the formation of the correct disulfide bonds: in the absence of this ion, oxidation of the modules yields multiple disulfide isomers, whereas folding in its presence leads to predominantly a single conformation (Atkins et al., 1998; Bieri et al., 1998). The calcium ions not only determine the outcome of folding, but also stabilize the conformation of the fully oxidized polypeptide: removal of the calcium results in a marked loss of 3D structure (Atkins et al., 1998). The requirement of calcium for proper folding and structural integrity has also been observed with LB_6 (North & Blacklow, 1999), the $LB_{1–2}$ concatemer (Bieri et al., 1998), the $LB_{5–6}$ concatemer (North & Blacklow, 1999), and two modules of the LRP complement-like domains, CR_3 and CR_8 (Dolmer et al., 1998; Huang et al., 1999). The crystal structure of LB_5 shows that the calcium ion is coordinated by the carboxyl groups of D196, D200, D206, and E207 and by the backbone carbonyls of W193 and G198 (Fass et al., 1997). An NMR titration study of the acidic residues of LB_1 (Atkins et al., 1998) suggested that a similar calcium ligand pattern is also extant in this module but E30, which corresponds to D196 in LB_5, was titratable and therefore may not participate in calcium binding in LB_1.

In a previous study, we found no substantial changes in the Cα-proton chemical shifts in the $LB_{1–2}$ concatemer from those of the individual modules (Bieri et al., 1998). This finding is paralleled by a recent study of another concatemer, $LB_{5–6}$, by $^1H–^{15}N$ heteronuclear single-quantum spectroscopy (North & Blacklow, 1999). The absence of significant changes in chemical shifts in these two concatemers suggested that the ligand binding modules of LDLR might be structurally independent of each other, but did not clarify the role of the linking residues.

We report here the first 3D structure of a concatemer of ligand-binding modules of human LDLR, $LB_{1–2}$. Although earlier experiments in which mutated LDLR was expressed in transfected COS cells led to the conclusion that the first and second cysteine-rich repeats are not necessary for interaction with apoB-100 or apoE (van Driel et al., 1987; Esser et al., 1988), more recent experiments indicate that these repeats do play an important role in lipoprotein binding (Sass et al., 1995; Rødningen et al., 1999). The structures of the individual modules within the $LB_{1–2}$ concatemer match those of the isolated modules (Daly et al., 1995a, 1995b), but inclusion of a larger number of restraints has led to a better definition of LB_2, and incorporation of explicit restraints for the calcium ion-binding ligands in the structural calculations has led to a refinement of segments of the calcium-binding loops of both modules. No intermodule NOEs were detected, indicating that these two modules are structurally independent. Their relative orientation is partly constrained by the linking tetrapeptide, but the lack of medium- and long-distance NOE restraints arising from this linker and the near random coil shifts of its backbone proton resonances suggest that it has substantial flexibility.

Results and discussion

Spin system assignment and secondary structure

Three-dimensional structure determination by homonuclear NMR spectroscopy methods is limited to molecules up to ~10 kDa (Evans, 1995), where peak overlap, ambiguity of cross peak assignments, and broader linewidths emerge as major problems. Despite these limitations, these methods have proven sufficient to solve high resolution structures of proteins up to ~11.5 kDa, provided that the cross peaks are well dispersed (Barthe et al., 1997; Bayer et al., 1998; De Morino et al., 1999). In this study, the standard homonuclear spectroscopy methods were also used to solve the solution structure of $LB_{1–2}$. The chemical shifts of $LB_{1–2}$ were well dispersed, as shown in the fingerprint region of the NOESY spectra, with the exception of a crowded area near 3.9–4.8 ppm in *F*1 and 8.1–8.9 ppm in *F*2 (Fig. 2). Spin systems were initially assigned in the TOCSY spectra with the aid of the published chemical shift data for the individual modules (Daly et al., 1995a, 1995b). These assignments were then mapped onto the NOESY spectra where the consistency of preliminary TOCSY assignments was verified by following Hα-HN($i, i + 1$) and HN-HN($i, i + 1$) connectivities. There were a number of similar chemical shifts observed in the NOESY spectra. In the fingerprint region, for example, NOE peak overlaps were observed between I19 HαHN and C74Hα-D75HN, and between S53 HαHN and E37 HαHN. However, most NOE peaks that were initially ambiguously assigned were later resolved either manually by measuring distances between possible atoms during structure refinement or with an aid of an automatic NOE assignment protocol using NOAH (Mumenthaler et al., 1997).

In contrast to most resonances, the amide proton chemical shifts of the linker residues, L43-S44-V45-T46, at 8.06, 7.98, 8.04, and 8.04 ppm, respectively, and the Cα-proton shifts, were close to their random coil values (Fig. 2). The chemical shifts of $LB_{1–2}$

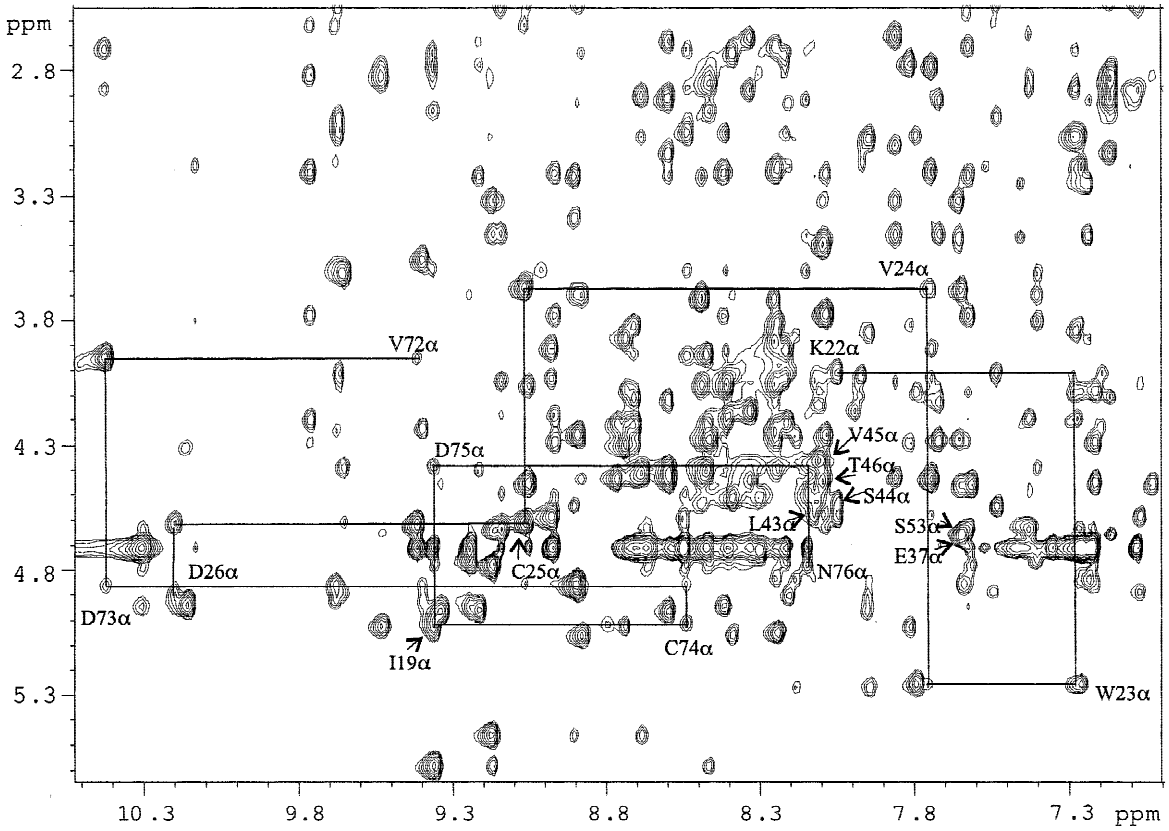

Fig. 2. The fingerprint region of $LB_{1–2}$ from a NOESY spectrum acquired at 310 K, pH 5.5. The demonstration of sequential assignments for the segments K22-W23-V24-C25-D26 (LB_1) and V72-D73-C74-D75-N76 (LB_2) are shown with connecting lines. NOE overlaps between I19 Hα-HN and C74 Hα-D75 HN, and between S53 Hα-HN and E37 Hα-HN, are indicated with arrows. The linker, L43-S44-V45-T46, amide protons have similar chemical shifts that are close to their random coil values.

resonances are available in Supplementary material in the Electronic Appendix (Table S1).

The majority of ^3J Hα-HN couplings observed in the DQF-COSY spectra were $>$7 Hz, and only two (Q14 and Y21) were $<$4 Hz. The presence of large coupling constants and a large number of strong Hα-HN ($i, i + 1$) NOEs indicates that the secondary structure of $LB_{1–2}$ is predominantly composed of β-strands and loops. There are several amide protons with slow or medium deuterium exchange rates in both modules of $LB_{1–2}$ (Fig. 3). Some of these protons were located within the β-hairpin structure, where in LB_1 the amide protons of residues F11, C13, and I19 were involved in hydrogen bonding with the backbone carbonyls of I19, K17, and F11, respectively (Daly et al., 1995b). However, the corresponding residues in LB_2 as part of the concatemer (F52, C54, and I62) were in fast exchange. The presence of 3_{10}-helical structure in both modules was indicated by C=O $\rightarrow$ NH ($i, i + 3$) hydrogen bonds (Wüthrich, 1986; Smith et al., 1996; Millhauser et al., 1997), namely W23 $\rightarrow$ S20 and V24 $\rightarrow$ Y21 in LB_1, and W66 $\rightarrow$ P63 and R67 $\rightarrow$ Q64 in LB_2, and one ^3J Hα-HN $<$ 4.0 Hz, for residue Y21. The short- and medium-range NOEs, coupling constants and amide exchange rates, are summarized in Figure 3.

Three-dimensional structure determination

The best 50 of the 100 structures generated from DYANA calculations (Güntert et al., 1997) were chosen as the input for X-PLOR molecular dynamics simulations. These calculations were performed excluding and including explicit restraints for calcium ion coordination, which resulted in only minor differences. The most notable changes were a decrease of the average Leonard–Jones van der Waals energy from -416.8 to -436.1 kcal/mol, a decrease of electrostatic energies from -8.0 to -18.7 kcal/mol and an increase of the average NOE restraint energy from 53.8 kcal/mol to 59.0 kcal/mol on inclusion of these restraints. The statistics of the NMR structures are shown in Table 1.

The overall structure of $LB_{1–2}$ is well defined, except for the N-terminal four residues (which include the Gly and Ser residues from the thrombin cleavage site) and the linker (Fig. 4). The C-terminal residues are more constrained because of the disulfide bond formed by the final residue. The inclusion of calcium in the molecular dynamics simulations did not significantly change the global structure, as reflected by the similarity of the angle order parameters in structures calculated including or excluding calcium. The inclusion did improve the quality of the structure, increasing the angle order parameters of backbone regions G27-S28 and Q71-E80 from an average of 0.78 to 0.96, and improving the definition of the side chains of the acidic residues that coordinate the calcium ion.

The backbone pairwise RMSD of LB_1 from C6–C42 is 0.47 $\pm$ 0.11 Å (1.14 $\pm$ 0.12 Å for all heavy atoms), and the pairwise RMSD of LB_2 from C47–C83 is 1.05 $\pm$ 0.24 Å (1.85 $\pm$ 0.33 Å for all heavy atoms). However, the family of structures did not super-

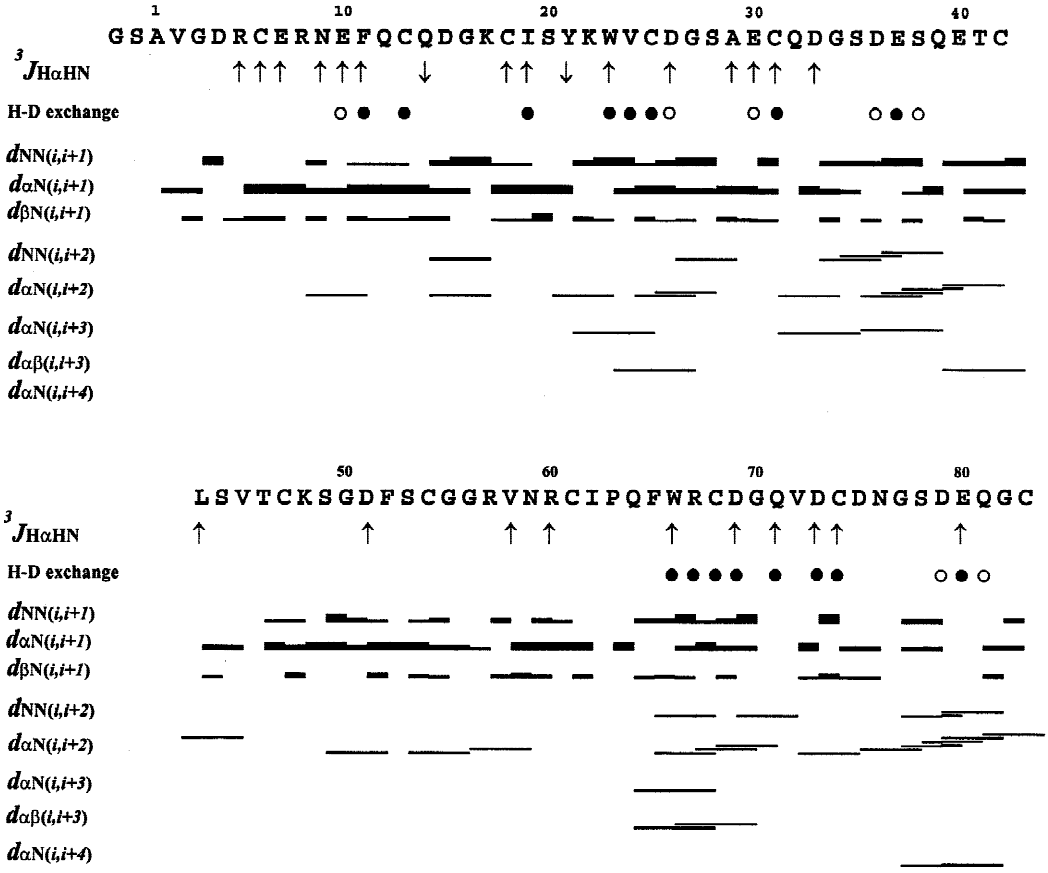

Fig. 3. Summary of short- and middle-range interactions in LB_{1-2}, showing NOE connectivities and ^3J Hα-HN coupling constants. Large and small ^3J Hα-HN coupling constants (>8 Hz and <4 Hz) are indicated with (↑) and (↓), respectively. Slow and medium amide proton exchange rates are shown with filled and open circles, respectively.

impose closely over their full length (backbone pairwise RMSD of 3.63 ± 1.54 Å) because the conformation of the L43–T46 segment that connects the two modules is not well defined (Fig. 5). Stereochemical quality assessment of the NMR structures by PROCHECK-NMR (Laskowski et al., 1996), showed that 65.6, 30.0, 3.9, and 0.6% residues were in the most favorable, additionally allowed, generously allowed and disallowed regions of the Ramachandran plot, respectively. However, when only well-defined regions (C6–C42 and C47–C85) were considered in the analysis, the number of residues in the most favorable, additionally allowed and generously allowed regions were 70.2, 26.4, and 3.4%, respectively, with none in the disallowed region. These latter figures are comparable to those presented in a recent survey of the quality of NMR structures (Doreleijers et al., 1998). There were few medium- or long-range NOEs or dihedral restraints involving the linker residues, resulting in low ϕ and ψ angle order parameters, which varied between 0.48–0.95 and 0.86–0.88, respectively. This paucity of restraints could have several origins including adoption of a small number of rapidly interconverting conformations, adoption of an extended conformation in which there will be few mid-range NOEs, or relatively unconstrained motion about the NH-Cα and Cα-C=O bonds. However, the combined evidence of near-random coil Cα- and amide proton chemical shifts, and the paucity of NOE restraints in such a small linker suggests that it may be mobile, allowing the two modules to rotate around the linker axis.

Structure description

The overall shape of LB_{1-2} can be described as an extended, globular molecule with a small but flexible region in the middle. The backbone folds of LB_{1-2} are similar to those of the individual modules. The secondary structures of both consist of a small β-hairpin structure (F11–I19 in LB_1 and F52–I62 in LB_2) followed by a short 3_{10}-helix (S20–V24 in LB_1 and P63–R67 in LB_2), a small loop near the Ca^{2+} binding region (C25–A29 in LB_1 and C68–V72 in LB_2) and successive turns (Fig. 6). The β-hairpin structure appears more flexible in LB_2 as there is no indication of slow amide proton exchange for residues F52, S53, C61, and I62. The 3_{10}-helix secondary structures in this concatemer are distorted, as indicated by the large ^3J Hα-HN couplings of W23, V24, and W66. The distortions of these helices from ideal geometry is a consequence of coordination of calcium ions by the carbonyl groups of the tryptophan residues and, in LB_2, the presence of a proline residue at the start of the helix.

A second 3_{10}-helix structure, which spans the conserved S-D-E sequence in LB_5 (Fass et al., 1997), was not detected in the corresponding region in LB_{1-2} (S35-D36-E39 and S78-D79-E80) during a secondary structure search using the classical Kabsch and Sander (1983) algorithm. However, the formation of 3_{10}-helix in these regions was highlighted by several strong HN-HN$(i, i + 1)$ and Hα-HN$(i, i + 2)$ NOEs (Fig. 2). The torsion angle values for

Table 1. *Summary of NMR restraints and X-PLOR structure statistics*

A. NMR restraints	
NOE distance restraints	
Total	889
Intraresidue	286
Sequential	273
Medium range (2–4)	184
Long range (>4)	146
Dihedral angle restraints	
Total	32
ϕ	26
χ_1	6
Backbone hydrogen bonds	13
Disulfide bonds	6
Calcium restraints[a]	12[a]

	With Ca^{2+}	Without Ca^{2+}
B. Quality of 20 lowest energy structures		
X-PLOR energies (kcal mol^{-1})[b]		
Vdw[c]	−436.1 ± 5.7	−416.8 ± 11.2
Electrostatic	−18.7 ± 0.8	−8.0 ± 1.1
NOE restraints	59.0 ± 3.5	53.8 ± 3.1
Dihedral restraints	0.1 ± 0.1	0.2 ± 0.1
RMSD from idealized covalent geometry		
Bonds	0.01 ± 0.01	0.01 ± 0.01
Angles	2.37 ± 0.04	2.39 ± 0.04
Impropers	0.21 ± 0.01	0.22 ± 0.01
Dihedrals	0.44 ± 0.16	0.55 ± 0.15
Average pairwise RMSD of Cartesian coordinates		
Backbone (N, Cα, C′)		
6–42	0.47 ± 0.11	0.65 ± 0.20
47–83	1.05 ± 0.24	1.08 ± 0.25
23–38	0.25 ± 0.08	0.55 ± 0.29
66–81	0.55 ± 0.17	0.71 ± 0.34
All heavy atoms		
6–42	1.14 ± 0.12	1.35 ± 0.18
47–81	1.85 ± 0.33	1.84 ± 0.32
23–38	0.75 ± 0.18	1.26 ± 0.27
66–81	1.32 ± 0.23	1.55 ± 0.35

[a]Calcium restraints included as NOE restraints for structures calculated with calcium coordination.
[b]Energy minimized structure using CHARMM force field.
[c]Leonard–Jones van der Waals energy.

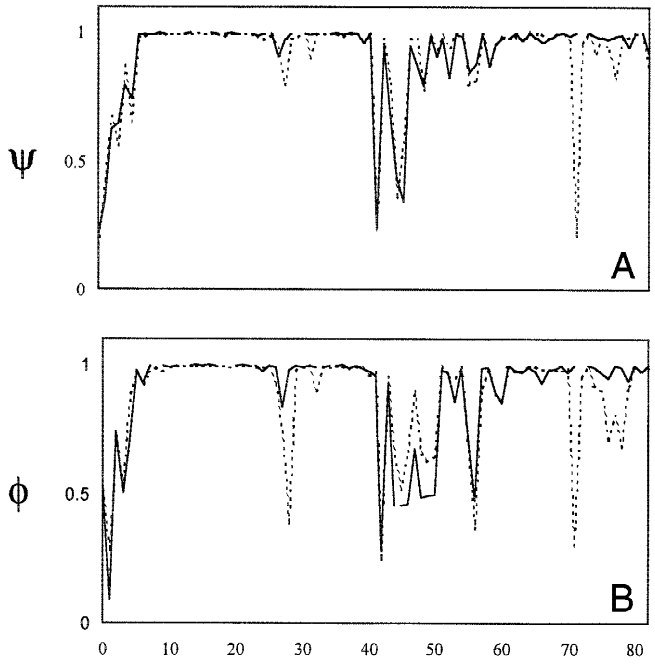

Fig. 4. (**A**) ψ and (**B**) ϕ order parameter plots for ensembles of the 20 lowest energy structures of $LB_{1–2}$, calculated with (solid line) or without (dotted line) calcium coordination restraints.

S35, D36, and E37 are −48.6 ± 3.1, −62.6 ± 1.7, −108.3 ± 9.4° (ϕ), and −58.6 ± 1.5, −18.9 ± 6.9, 2.3 ± 1.4° (ψ), respectively; and for S78, D79, and E80 −73.9 ± 3.7, −125.4 ± 8.2, −121.5 ± 20.3 (ϕ), and −23.2 ± 8.5, −6.8 ± 20.5, −58.7 ± 4.1 (ψ), respectively. These values, except for residues D79 and E80, are close to the range of most populated 3_{10}-helix torsion angles, which have a broad range with mean values of −62.8 ± 38.0° and −16.5 ± 34.7°, for ϕ and ψ angles, respectively (Smith et al., 1996). The SDE segments of $LB_{1–2}$ contain only a few HN → C=O ($i, i + 3$) hydrogen bonds, which are an essential feature of 3_{10}-helices (Kabsch & Sander, 1983). In LB_1 these hydrogen bonds are present at E37 → G34 and S38 → S35. However, the SDE segment of LB_2 contains a mixture of ($i, i + 3$) and ($i, i + 4$) hydrogen bonds, namely E80 → G77 and D81→ D77, and thus does not meet the normal criteria for classification as a 3_{10}-helix.

Superimposition of the backbone heavy atoms of the NMR structures of LB_1 (Daly et al., 1995b) and LB_2 (Daly et al., 1995a) onto corresponding sections of the lowest energy $LB_{1–2}$ structure obtained without explicit inclusion of calcium ions resulted in pairwise RMSD values of 2.22 and 2.63 Å, respectively (Fig. 7A,B). The LB_2 structure in $LB_{1–2}$ is better defined than that obtained earlier for the single module (Daly et al., 1995a) as a result of the use of a higher number of NOE and dihedral angle restraints. Comparison of LB_5 with the structures of the concatemer modules LB_1 and LB_2 obtained with inclusion of calcium restraints resulted in average pairwise RMSD values of 1.17 and 1.89 Å, respectively (Fig. 7C,D). The concatemer LB_1 and LB_5 differ at the C-terminus (S38–C42) because of the insertion of two extra amino acids, E40 and T41 in LB_1. Similarly, LB_5 and the concatemer LB_2 differ in the β-hairpin structure because of the insertion of R57 and V68 in the latter. These values reinforce the qualitative conclusion, reached on the basis of chemical shift differences, that the structure of the repeats is uninfluenced by linking them in the concatemer.

The calcium ion-binding site

The crystal structure of LB_5 (Fass et al., 1997) revealed that the calcium ion was protected from the solvent and was coordinated with four carboxyl and two backbone carbonyl groups (the latter indicated by ‡ and † in Fig. 1). By sequence comparison with LB_5, calcium coordination in $LB_{1–2}$ is anticipated to be to W23 (‡), D26, S28 (†), E30, D36, and E37 in LB_1, and to W66 (‡), D69, Q71 (†), D73, D79, and E80 in LB_2 (Fig. 1). The four charged side chains are partly within the "core" of each LB module, rather than being

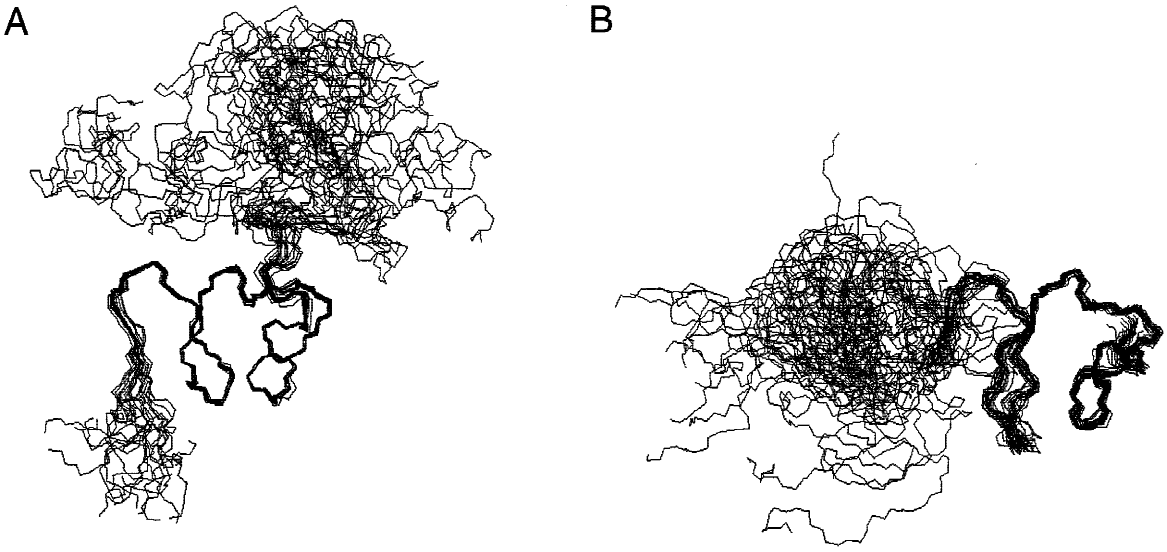

Fig. 5. Superimposition of 20 NMR-derived structures of calcium-coordinated LB_{1-2}. (**A**) Structures were superimposed over the backbone of residues C6–C42 (LB_1) or (**B**) of residues C47–C83 (LB_2). The NMR structures are not superimposable across the whole molecule because the linker between the two modules is flexible.

completely exposed to the solvent. Each of these acidic residues contributes one partially negatively charged carboxyl oxygen for calcium ligation, with the residual charge on the second, free carboxyl oxygen contributing to the local negative surface potential.

This coordination reduces the response of these carboxyl groups to pH changes compared with solvent-exposed residues, a phenomenon that was detected by NMR spectroscopy as reduced pH-dependent chemical shift variations of the corresponding β- and γ-protons (Atkins et al., 1998). In this titration study of LB_1 over pH 3.9 to 6.9, the β- and γ-proton chemical shifts of solvent-exposed residues E7 and D15 moved by >0.10 ppm, whereas the β-proton resonance of the buried D36, shifted by only 0.02 ppm (Atkins et al., 1998). In our studies of recombinant LB_2, comparison of chemical shifts at pH 4.5 and 7.5 (Table 2) revealed that the β- and γ-protons of residues D73, D79, and E80 have small changes (up to 0.03 ppm), consistent with their being solvent-protected calcium ligands. The side-chain protons of E30, D26 and its equivalent residue in LB_2, D69 (Table 2), exhibited shifts of $\sim$0.04–0.09 ppm with pH, indicating that these residues are partially exposed to the solvent.

The calcium binding regions of LB_1 (W23–E30 and S35–E37), LB_2 (W66–D73 and S78–E80), and LB_5 (W193–D200 and S205–E207) have similar structures. The majority of amino acid side chains in these regions, excluding the calcium-binding residues, are exposed to the solvent. In LB_5, residue P199, which is located between the third and fourth calcium binding ligands, D198 and

Fig. 6. MOLMOL schematic diagram (Koradi et al., 1996) of the lowest energy structure of LB_{1-2}, showing the backbone Cα trace, β-hairpins (ribbon with arrow), 3_{10}-helices, and calcium ions (dark spheres).

Table 2. *pH dependence of the chemical shifts of acidic residues near the calcium binding site*

	Chemical shifts (ppm)		$\lvert\Delta\rvert$
Residue LB_1	pH 4.4	pH 6.9	(ppm)
D26[a,b]	2.45	2.38	0.07
	3.15	3.11	0.04
E30[a,b]	1.93	1.84	0.09
	2.08	2.15	0.07
D36[a,b]	2.55	2.54	0.01
	2.78	2.76	0.02
E37[a,b]	1.91	1.90	0.01
	2.53	2.54	0.01
LB_2	pH 4.5	pH 7.5	
D69[b]	2.70	2.63	0.07
	3.26	3.18	0.08
D73[b]	2.79	2.79	0.00
	2.97	3.00	0.03
D79[b]	2.64	2.61	0.03
	3.05	3.03	0.02
E80[c]	2.10	2.11	0.01

[a] Chemical shift data from Atkins et al. (1998).

[b] Chemical shifts of $\beta\beta'$ or $\gamma\gamma'$ protons of the corresponding aspartate or glutamate residues.

[c] Chemical shift of degenerate γ protons.

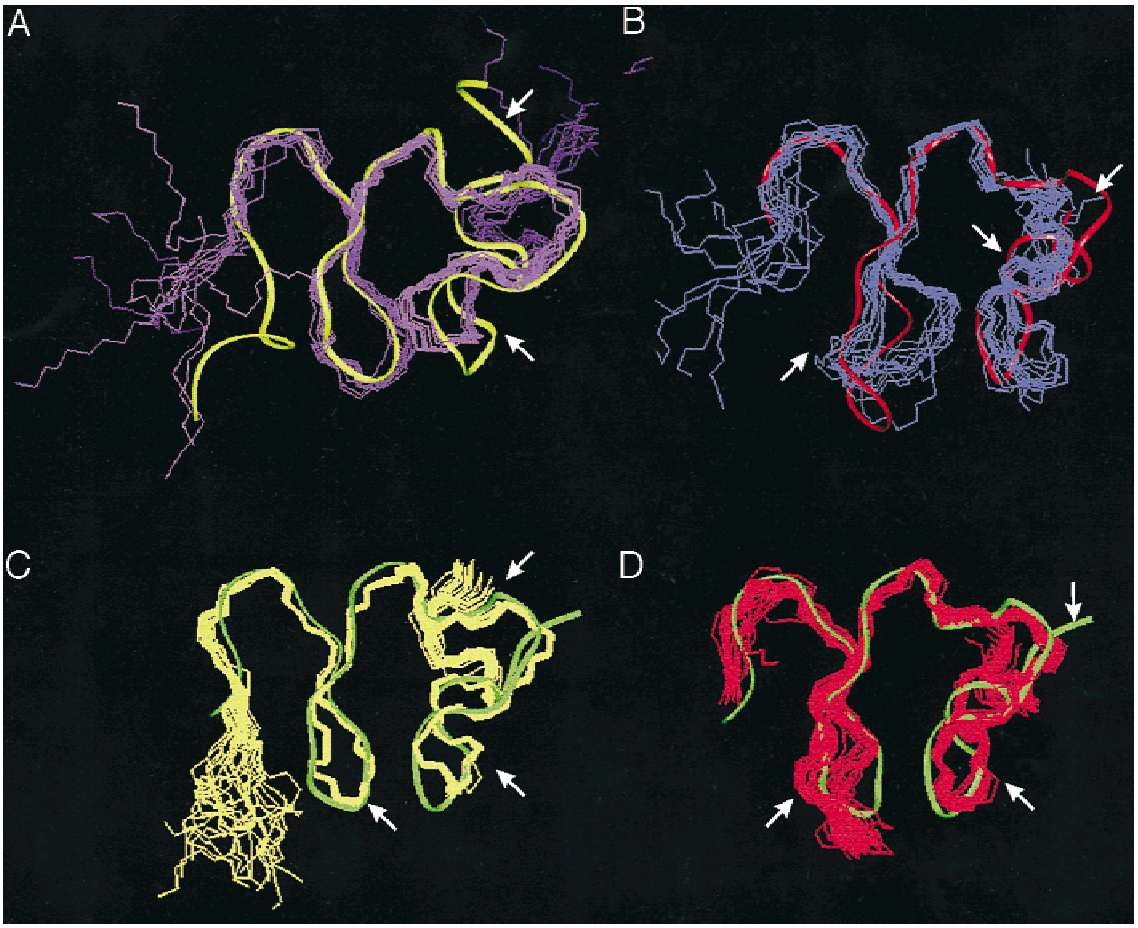

Fig. 7. Superimposition of the backbone heavy atoms of the lowest energy $LB_{1–2}$ concatemer structure (cLB_1 and cLB_2) with the NMR structures of the individual modules LB_1 and LB_2 (Daly et al., 1995b, 1995a), and with the crystal structure of LB_5 (Fass et al., 1997). **A:** Superimposition of LB_1 (red) and cLB_1 (yellow) calculated without explicit calcium restraints (average pairwise RMSD 2.22 Å). **B:** Superimposition of LB_2 (purple) and cLB_2 (red) calculated without explicit calcium restraints (average pairwise RMSD 2.63 Å). **C:** Superimposition of LB_5 (green) and the family of concatemer LB_1 module structures (yellow) calculated with explicit calcium restraints (average pairwise RMSD 1.17 Å). **D:** Superimposition of LB_5 (green) and the family of concatemer LB_2 structures (red) calculated with explicit calcium restraints (average pairwise RMSD 1.89 Å). Regions with divergent structures are indicated by arrows.

D200, also has its side-chain ring exposed to the solvent, as do the similarly placed residues in LB_1 and LB_2, A29 and V72. By contrast, the orientation of the side chain of tryptophan residue W23 differs from W66 and W193. The indole group of W23 (LB_1) is partly exposed to the solvent, revealing the carboxyl group of E30 (Fig. 8, LB_1), whereas the indole groups of W66 (LB_2) and W193 (LB_5) function as a "lid" on the calcium binding site, being sterically constrained by the side chains of P63 and F65 (Fig. 8, LB_2) or H190 (LB_5). The importance of these indole groups is highlighted by the familial hypercholesterolemia that accompanies mutation of W66 to glycine (Moorjani et al., 1993; Jensen et al., 1996).

It appears that these differences in the orientation of the indole groups make the carboxyl group of E30 more solvent accessible compared to D73 and D200, which may account to the greater sensitivity of E30 in LB_1 to pH changes (Atkins et al., 1998) and also for the differences in calcium ion binding between LB_1 and LB_2. On the other hand, LB_1, LB_2, and LB_5 all have acidic residues (D36, D79, and D206) that are completely buried within the calcium binding site. The side chains of the C-terminal calcium ligands of each of these modules, E37, E80, and E207, restrict access of solvent to the Ca^{2+} ion. A closer examination of the calcium binding sites of the three modules (Fig. 8) shows very similar orientations of the backbone carbonyl groups (W23, S28, W66, Q71, W193, and G198). However, the orientations of the acidic groups of LB_1 and LB_2 were not similar, with E80 having a particularly low χ^2 angle order parameter, and did not form the perfect tetrahedral structure shown in the crystal structure of LB_5. Although these differences may reflect some flexibility of calcium coordination in solution, they may also arise from the more limited information obtained from ^{1}H NMR spectroscopy for the calcium ion site compared with X-ray crystallography.

From the studies of LB_1, LB_2, LB_5, and CR_8, it is likely that the consensus for the third calcium ligand in the sequence of the LB-like modules is the backbone carbonyl group of a nonconserved residue placed midway between two acidic residues that bind through their side chains. Across the spectrum of modules depicted in Figure 1, this residue is also often D or E, but it is S and Q in $LB_{1–2}$, and G in LB_5. The high affinity of LB_5 for calcium ions suggests that the nature of the side chain of this residue does

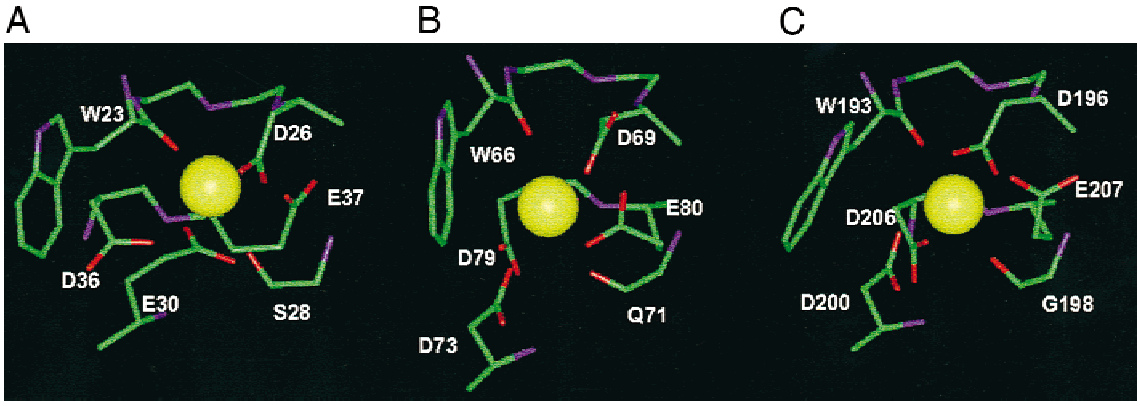

Fig. 8. Comparison of calcium binding sites of the lowest energy NMR structure of (**A**) LB_1, (**B**) LB_2, and the crystal structure of (**C**) LB_5. The carbon, nitrogen and oxygen atoms are shown in green, blue, and red, respectively. The most pronounced differences in the calcium binding sites are the differences in orientation of the indole groups of the tryptophan residues, the side chain of residue E30 compared to D73 and D200, and the C-terminal ligands E37, E80, and E207. These figures were created using Insight98 (Molecular Simulations Inc.).

not exert a strong influence on ion binding. Calcium coordination by a nonconserved backbone carbonyl was also observed in the crystal structure of human prosarin S100A7 (Brodersen et al., 1999), where the fourth calcium ligand is the carbonyl of K68. However, unlike LB_1, LB_2, and LB_5, the fifth ligand of prosarin is a water molecule, which is coordinated by the carboxyl group of D77.

Structural flexibility

A number of NOEs between the LB_1 hydrophobic residue pairs F11–I19, F11–V24, I19–V24, I19–W23, I19–V24, and W23–V24 were observed. In LB_2, similar pairwise interactions were observed: F52–I62, I62–W66, P63–W66, P63–F65, and F65–W66. Within each module, these residues have been shown to constitute a small hydrophobic core (Daly et al., 1995a, 1995b). However, there were no observable intermodule NOEs between these hydrophobic regions, and they therefore do not appear to interact with each other in the concatemer.

The concatemer $LB_{1–2}$ retains the structure of each individual module, and the linker allows these modules to alter their relative orientations. However, the movement of the linker is not completely free as indicated by the presence of a large ^3J Hα-HN coupling (>8.0 Hz) for residue L43. It appears from the family of 20 NMR structures that there is a weak preference for the two domains to take up a mutually perpendicular orientation. The flexibilities observed within the concatemers $LB_{1–2}$ and $LB_{5–6}$ could be mirrored in the residues linking the other modules, with potentially the greatest flexibility between LB_4 and LB_5, resulting from the 12-residue linker at this point. It is possible that flexible orientations of the LB modules are essential for the LDLR to accommodate such diverse ligands as apoE and apoB-100.

Both flexible and restrained orientations between other independently folded domains have been reported (Campbell & Downing, 1998). For example, the NMR structure of the 162-residue, calcium-binding protein skeletal muscle troponin C (Slupsky & Sykes, 1995) showed that the orientation of one domain with respect to the other is not well defined. These two modules are connected by a nine-residue linker in which only three residues (86–88) are highly flexible. On the other hand, a concatemer of the two calcium-binding EGF-like domains of human fibrillin-1 exhibited a rigid, rod-like arrangement (Downing et al., 1996). In contrast to $LB_{1–2}$, in which calcium-binding is not shared, the calcium binding site in fibrillin-1 is located between the two domains and, together with hydrophobic interactions, it stabilizes the concatemer structure.

Surface properties

In LB_1 one face is rich in polar residues, including the charged residues D4, R8, E7, E10, K17, K22, and fractional charges from the partially solvent-protected, calcium-binding carboxyl groups of D26, E30, D36, and E37 (Fig. 9A,B). The equivalent face in LB_2 has D51, R57, R60, D75, and partial charges from D69, D73, D79, and E80 (Fig. 9B,C). The second face has a small surface with low electrostatic potential, containing two small hydrophobic patches of the aromatic F11 and F52 and only a few polar residues, R5, E7, and E40 in LB_1 (Fig. 9C), and K48, R57, and R67 in LB_2 (Fig. 9D).

The polar residues, D15 and R57, are located in the middle of the β-hairpin structures, whereas D33 and D75 are in similar locations in the middle of the calcium-binding loops. The presence of negatively charged residues in these large loops may be of structural or functional importance: in the crystal structure of LB_5 this β-hairpin and its parallel, C-terminal loop are stabilized by hydrogen bonding between the carboxyl group of E187 and the amide backbones of E187 and K202, and also between the carboxyl group of D203 and the backbone amide of S185. If hydrogen bonds involving D33, D75, or Q76 were involved in such structural stabilization, one would expect to find slow or medium amide proton exchange rates in the corresponding regions of $LB_{1–2}$: none were observed, but the invariance of the chemical shifts of the side chain protons of D33 and D75 with pH does suggest that their carboxyl groups are involved in hydrogen bonding. On the other hand, D33, D75, and D203 may also be functionally important: this Asp residue is conserved across all seven LB modules (shifted by one residue in LB_2) and both complement repeats, CR_3 and CR_8, and as they are not involved in calcium coordination they could participate in lipoprotein binding.

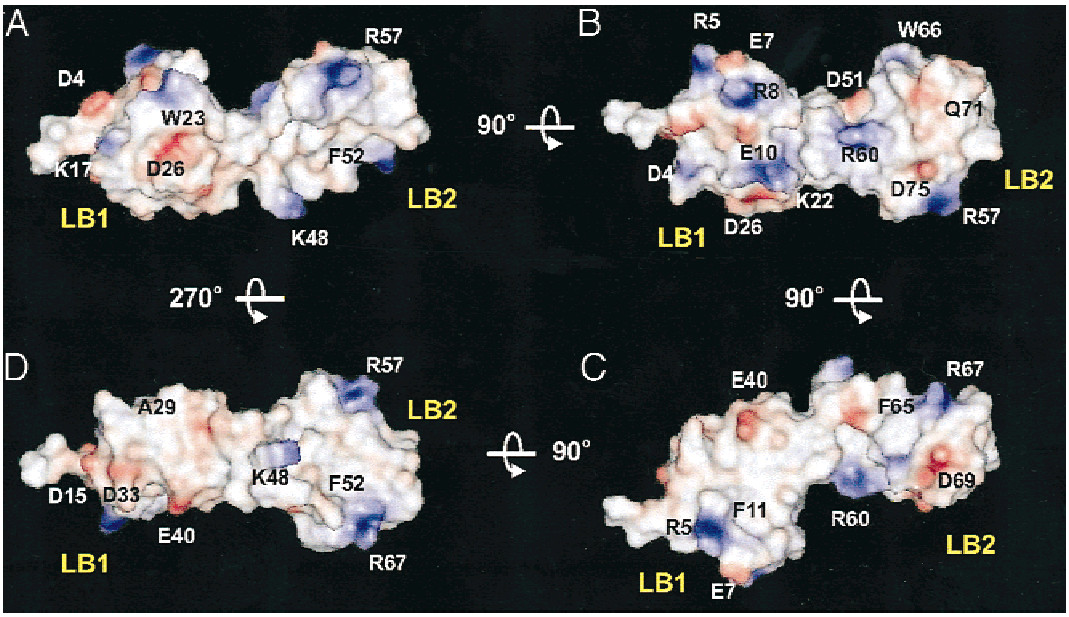

Fig. 9. Electrostatic surface potential of $LB_{1–2}$. The orientation of this molecule is, at left (**A**), similar to that in Figure 6. **B**, **C**, and **D** were produced by sequential 90° rotations of the molecule in **A** around the horizontal axis. The surface contour was calculated using solvent accessibility. Red and blue indicate surfaces with negative and positive partial charge, respectively. This diagram, which presents the lowest energy structure as in Figure 6, was generated using WebLab ViewPro (Molecular Simulations Inc.).

As noted by Huang et al. (1999), although the folds of the LB modules are similar the overall sequence identity is only about 15 of 40 residues, with the majority of these conserved residues forming disulfide bonds or acting as calcium ion ligands. Within this basic framework, there are such changes between LB_1 and LB_2 as the lengthening of the β-hairpin structure in LB_2 resulting from the insertion of R57 and V58, and many changes in charged and hydrophobic surface residues including E7 to K48, Y21 to Q64, K22 to F65, V24 to R67, and Q32 to D75. Such variations, which are evident also in LB_5 and CR_8 (Huang et al., 1999), give each module a distinctive signature that may determine its part in the complex interactions with the lipoproteins.

Lipoprotein binding

It was initially proposed that the LDLR bound its several ligands predominantly through a calcium-dependent interaction between its acidic side chains and the basic residues on the apolipoproteins (Wilson et al., 1991). It is now clear from the known 3D structures that the acidic residues of each module that coordinate the calcium ion are buried in the binding site and are therefore unavailable for interaction with lipoproteins, i.e., their role is in maintenance of the polypeptide fold, as shown by the profound effects of calcium ion removal on the 3D structure (Daly et al., 1995a; Atkins et al., 1998). Assuming conservation of the calcium-binding ligands, there are a number of remaining acidic groups (6, 2, 4, 2, 4, 4, and 6 in LB_1 to LB_7, respectively) that are still available for interaction with their lipoprotein ligands.

In addition to ionic interactions, LB_1, LB_2, and LB_5 each have a face that could participate in hydrophobic interactions. This face could be utilized in ligand binding or in arrangement of the cysteine-rich repeats in the intact binding domain. In this regard, we note that none of the LBs nor the concatemer we have studied has a strong tendency to form dimers and consequently if hydrophobic interactions do play a part in maintaining an ordered arrangement of the seven repeats other forces are likely to contribute significantly. For the modules we and others have studied to date, LB_1 (Daly et al., 1995b), LB_2 (Daly et al., 1995a), LB_5 (Fass et al., 1997), LB_6 (North & Blacklow, 1999; D. Clayton, I.M. Brereton, P.A. Kroon, & R. Smith, unpubl. obs.), LB_7 (B. Hawkins & R. Smith, unpubl. data), $LB_{1–2}$ (this work), $LB_{5–6}$ (North & Blacklow, 1999), and $LB_{1–7}$ (Simmons et al., 1997), it seems that inter-module interactions are unnecessary for adoption of the correct polypeptide fold. Moreover, although it has been considered that the shortness of the linkers, 4–5 residues, between most of the modules might lead to stacking of the repeats with perhaps a loop between repeats 4 and 5 (Brown et al., 1997), this idea is not supported by the observations on the concatemers. Their linkers, although short, still allow considerable freedom of rotation of the successive modules although their size does perhaps preclude folding back of adjacent modules that might allow extensive interactions between them. The concept that the 3D arrangement of all seven modules is critical for recognition of the apolipoproteins is also belied by the extensive mutagenesis studies in which mutation or deletion of single repeats diminished, but did not eliminate, lipoprotein-receptor interactions (van Driel et al., 1987; Esser et al., 1988; Russell et al., 1989). The current studies are thus consistent with the "beads on a string" model for the ligand binding domain.

Materials and methods

Protein expression, folding, and purification

The sequences encoding LB_2 and $LB_{1–2}$ were separately cloned into the vector pGEX-2T (Pharmacia, Uppsala, Sweden) and transformed into *Escherichia coli* DH5α cells (Bieri et al., 1995a, 1998).

Transformed cells were grown in 2× yeast tryptone medium (Amyl Media, Melbourne, Australia) containing 20 mg/mL ampicillin at 37 °C, pH 7.0 and induced at $A_{600} = 1.2$ with 0.2 mM isopropyl-β-D-thiogalactopyranoside for 2 h. The cells were centrifuged at 5,000 *g*, at 4 °C for 20 min, then resuspended in phosphate-buffered saline (PBS; 30 mL per 1 L culture) containing 0.1 mM phenyl-methylsulfonyl fluoride and lysed using a French pressure cell operated at 800 psi. The lysate was incubated with 1% Triton-X100 for 30 min at 4 °C, then centrifuged at 15,000 *g* for 20 min. The supernatant was mixed with Zymatrobe glutathione beads (Department of Biochemistry, La Trobe University, Melbourne, Australia) for 1 h at 4 °C. After washing with PBS, the beads were incubated with 2 mM dithiothreitol and the immobilized fusion protein cleaved with thrombin (5 U/mg protein) for 2 h at room temperature. The cleaved LB_2 or concatemer was eluted with PBS.

The crude LB_2 and $LB_{1–2}$ were folded in the presence of 2.5 mM $CaCl_2$, 3 mM reduced glutathione, and 0.3 mM oxidized glutathione at 4 °C overnight (Bieri et al., 1998). They were purified using a BioCAD 700E (Perkin-Elmer, Foster City, California) with a R2 Poros 4 × 50 mm column (PerSeptive Biosystems, Framingham, Massachusetts) with a 5–35% acetonitrile gradient in 0.1% trifluoroacetic acid (TFA) over 15 min at 5 mL/min. The proteins were further purified using a Vydac C18 5 × 250 mm column (Hysperia, California) with a 20–35% acetonitrile gradient in 0.1% TFA over 30 min at 1 mL/min. Fractions containing LB_2 and $LB_{1–2}$ were lyophilized and the purified proteins analyzed by electrospray mass spectroscopy and polyacrylamide gel electrophoresis in the presence of sodium dodecyl sulfate (Bieri et al., 1998).

NMR experiments

For NMR spectroscopy, samples contained ~1.5 mM protein and 20 mM $CaCl_2$ at pH 5.5 and 6.0 in 5% or 99.9% D_2O (Sigma, St. Louis, Missouri). NMR experiments were performed on a Bruker DMX750 spectrometer (Bruker, Karlsruhe, Germany) at 300 and 310 K. TOCSY experiments (Braunschweiler & Ernst, 1983) were performed with 40, 80, and 120 ms MLEV-17 spin-lock sequences (Bax & Davis, 1985). NOESY experiments (Jeener et al., 1979) were performed with 100 and 250 ms mixing times. Water suppression was achieved using the WATERGATE method, incorporating a 3-9-19 refocussing pulse sequence with pulsed field gradients of ~100 mT/m (Piotto et al., 1992; Sklenar et al., 1993).

Typically, TOCSY and NOESY experiments were acquired into 1K complex data points, with 32 or 64 transients (respectively), over 500–600 F1 increments. Sine-bell window functions, shifted by $\pi/2$ in F2 and $\pi/4$ in F1, were applied to the data prior to Fourier transformation and baseline correction. DQF-COSY (Rance et al., 1983; Derome & Williamson, 1990) and E-COSY (Griesinger et al., 1987) spectra were typically acquired into a 2K × 512 complex data matrix that was zero-filled to 8K × 2K and multiplied by $\pi/2$-shifted sine-bell functions prior to Fourier transformation. ^3J coupling constants were extracted by fitting COSY multiplets with the Lorentzian lineshape fitting routine of the AURELIA program (Bruker). The hydrogen-deuterium exchange of the amide protons was examined with a series of short 1D-NMR spectra during the first hour, followed by a series of short TOCSY (16 transients, 200 F1 increments) for the next 12 h. Fast, medium, and slowly exchanging amide protons were classified based on the disappearance of signals after 20 min, 3 h, and 12 h, respectively. The calcium binding site of LB_2 was analyzed by comparing the β- and γ-proton chemical shifts of acidic residues of TOCSY spectra acquired at pH 4.5 and 7.5 at 310 K.

NMR assignments

NMR spectra were analyzed using XWINNMR (Bruker) and XEASY (Xia and Bartels, ETH-Zürich, Zürich, Switzerland). The spin systems were assigned by following Hα-HN($i, i + 1$) and HN-HN($i, i + 1$) connectivities (Wüthrich, 1986). NOESY spectra were assigned manually and also with the assistance of an automatic NOESY assignment program, NOAH (Mumenthaler et al., 1997). Resonances that initially could not be assigned unambiguously were excluded during preliminary structure calculations: they were gradually introduced during the refinement of NMR structures, as the ambiguity was resolved.

Structure calculations

The majority of distance restraints used in structure calculations were derived from 100 ms NOESY spectra. NOE peaks were picked manually and integrated using the XEASY peak picking and integration module, employing an elliptical integration area. NOE volumes were converted to upper-limit distances using the CALIBA macro of DYANA-1.5 (Güntert et al., 1997), and assigned as strong, medium, weak and very weak for upper bounds of 2.7, 3.5, 5.0, and 6.0 Å (for NOE peaks that were observed only in 250 ms NOESY spectra), respectively. Overlapped peaks were reclassified into weaker upper bounds before being introduced during structure refinement. A total of 889 NOE restraints (286 intraresidue, 273 short range, 184 medium range, and 146 long range), 26 Hα-HN torsion angle restraints, 6 Hα-Hβ torsion angle restraints, and 6 covalent disulfide bonds (C8–C20, C15–C33, C27–C44, C49–C63, C56–C76, and C70–C85; Bieri et al., 1995a, 1995b) were used as the inputs for structure calculations.

Initially, the structures were calculated without including implicit backbone hydrogen bonds as restraints. From these structures the H-bond acceptors were identified, permitting inclusion of 13 backbone hydrogen bond restraints (NH → C=O), namely, 11 → 19, 13 → 17, 19 → 11, 23 → 20, 24 → 21, 25 → 36, 37 → 34, 38 → 35, 66 → 63, 67 → 64, 68 → 79, 71 → 69, and 81 → 77. Hydrogen bonds were simulated as NOE restraints, where the distance between an amide proton and a carbonyl oxygen was restrained to be between 1.8 to 2.0 Å and the distance between an amide nitrogen and a carbonyl oxygen was restrained to lie between 2.7 and 3.0 Å (Williamson et al., 1985). The ϕ dihedral angle restraints for residues with ^3J Hα-HN > 8.0 Hz were set to 120 ± 40°. Stereospecific assignments were made based on ^3J Hα-Hβ coupling constants and HN-Hβ/Hα-Hβ NOE patterns (Clore & Gronenborn, 1993), resulting in χ^1 dihedral angle restraints that were set to −60 ± 30° for residues D51, C61, and C74, 60 ± 30° for D79, and −180 ± 30° for C20 and C68.

Initially, 100 structures were calculated using the torsion-angle dynamics and simulated annealing calculation program, DYANA. A total of 10,000 steps of torsion angle dynamics were performed for each calculation. The 50 structures from the DYANA calculations with the lowest target function ($f < 10$) were imported into X-PLOR (Brünger, 1992) for further simulated annealing and energy minimization.

Calcium ion coordination was simulated using distance restraints derived from the LB_5 crystal structure (Fass et al., 1997) following a procedure similar to that described by Kay et al. (1991).

Using the NMR titration data of LB_1 (Atkins et al., 1998) and LB_2, and by sequence homology to LB_5 (Fass et al., 1997), the calcium ion in LB_1 was assumed to be bound to the backbone carbonyls of W23 and S28, and the side-chain carboxyls of D26, E30, D36, and E37; and in LB_2 by the carbonyls of W66 and Q71 and the carboxyls of D69, D73, D79, and E80. The distances between the calcium ion and the carbonyl oxygens or the coordinating carboxyl oxygens were restrained as noncovalent bonds to 2.50 Å. No tetrahedral geometrical forces for calcium coordination were used in the calculation.

The X-PLOR simulations at 1,000 K were performed over 18 ps with geometrical force fields. The force constants for the NOE, hydrogen bond, and calcium restraints were 50 kcal mol^{-1} $Å^{-2}$ and 200 kcal mol^{-1} rad^{-2} for the dihedral angles. Structures were cooled to 0 K over a further 18 ps of dynamics. The resulting structures were energy minimized with the inclusion of electrostatic potentials using the CHARMM force field (Brooks et al., 1983) employing 2,000 steps of the Powell algorithm. The acceptance criteria for the NMR structures were: no single NOE violation >0.4 Å, no single dihedral angle violation $>5°$, and RMSD from the idealized bonds and angles of <0.01 Å and 3°, respectively.

NMR structures were analyzed and displayed using MOLMOL 2.6 (Koradi et al., 1996), Insight98 and WebLab Viewer Pro (Molecular Simulations, San Diego, California). Secondary structures were assessed using CalcSecondary module within the MOLMOL program, which utilizes Kabsch and Sander algorithm. PROCHECK-NMR (Laskowski et al., 1996) was used to assess the stereochemical quality of the structures.

Supplementary material in the Electronic Appendix

^{1}H resonance (Table S1) and hydrogen-bond (Table S2) assignments of LB_{1-2}.

Acknowledgments

We thank Dr. Bernadette Hawkins for helpful discussions, and Ms. Maria Caldiera and Mr. Lyle Carrington for assistance with protein purification. This work was supported by a grant to PAK, RS and IMB from the Australian National Health and Medical Research Council. Structure coordinates were deposited in the RSCB database under accession number 1F54.

References

Atkins AR, Brereton IM, Kroon PA, Lee HT, Smith R. 1998. Calcium is essential for the structural integrity of the cysteine-rich, ligand-binding repeat of the low-density lipoprotein receptor. *Biochemistry 37*:1662–1670.

Barthe P, Yang YS, Chiche L, Hoh F, Strub MP, Guignard L, Soulier J, Stern MH, Tilbeurgh HV, Lhoste JM, et al. 1997. Solution structure of human $p8^{MTCP1}$, a cysteine-rich protein encoded by the MTCP1 oncogene, reveals a new α-helical assembly motif. *J Mol Biol 275*:801–815.

Bax A, Davis DG. 1985. MLEV-17-based two-dimensional homonuclear magnetization transfer spectroscopy. *J Magn Reson 65*:355–360.

Bayer P, Arndt A, Metzger S, Mahajan R, Melchior F, Jaenicke R, Becker J. 1998. Structure determination of the small ubiquitin-related modifier SUMO-1. *J Mol Biol 280*:275–286.

Bieri S, Atkins AR, Lee HT, Winzor DJ, Smith R, Kroon PA. 1998. Folding, calcium binding, and structural characterization of a concatemer of the first and second ligand-binding modules of the low-density lipoprotein receptor. *Biochemistry 37*:10994–11002.

Bieri S, Djordjevic JT, Daly NL, Smith R, Kroon PA. 1995a. Disulfide bridges of a cysteine-rich repeat of the LDL receptor ligand-binding domain. *Biochemistry 34*:13059–13065.

Bieri S, Djordjevic JT, Jamshidi N, Smith R, Kroon PA. 1995b. Expression and disulfide-bond connectivity of the second ligand-binding repeat of the human LDL receptor. *FEBS Lett 371*:341–344.

Braunschweiler L, Ernst RR. 1983. Coherence transfer by isotropic mixing: Application to proton correlation spectroscopy. *J Magn Reson 53*:521–528.

Brodersen DE, Nyborg J, Kjeldgaard M. 1999. Zinc-binding site of an S100 protein revealed. Two crystal structures of Ca^{2+}-bound human psoriasin S100A7 in the Zn^{2+}-loaded and Zn^{2+}-free states. *Biochemistry 38*:1695–1704.

Brooks B, Bruccoleri R, Alafson B, Swaminathan S, Karplus M. 1983. CHARMM: A program for macromolecular energy, minimization, and molecular dynamics calculations. *J Comp Chem 4*:187–217.

Brown MS, Goldstein JL. 1986. A receptor-mediated pathway for cholesterol homeostasis. *Science 232*:34–47.

Brown MS, Herz J, Goldstein JL. 1997. LDL-receptor structure. Calcium cages, acid baths and recycling receptors. *Nature 388*:629–630.

Brünger AT. 1992. *X-PLOR manual version 3.1*. New Haven, CT: Yale University Press.

Campbell ID, Downing AK. 1998. NMR of modular proteins. *Nat Struct Biol 5*:496–499.

Clore G, Gronenborn A. 1993. In: Clore G, Gronenborn A, eds. *Topics in molecular and structural biology*. Basingstoke, England: Macmillan.

Daly NL, Djordjevic JT, Kroon PA, Smith R. 1995a. Three-dimensional structure of the second cysteine-rich repeat from the human low-density lipoprotein receptor. *Biochemistry 34*:14474–14481.

Daly NL, Scanlon MJ, Djordjevic JT, Kroon PA, Smith R. 1995b. Three-dimensional structure of a cysteine-rich repeat from the low-density lipoprotein receptor. *Proc Natl Acad Sci USA 92*:6334–6338.

De Morino S, Morelli MAC, Fraternalli F, Tomborini E, Musco G, Vrtala S, Dolecek C, Arosio P, Valenta R, Pastore A. 1999. An immunoglobulin-like fold in a major plant allergen: The solution structure of Phl p 2 from timothy grass pollen. *Structure 7*:943–952.

Derome A, Williamson M. 1990. Rapid-pulsing artifacts in double-quantum-filtered COSY. *J Magn Reson 88*:177–185.

Dolmer K, Huang W, Gettins PG. 1998. Characterization of the calcium site in two complement-like domains from the low-density lipoprotein receptor-related protein LRP and comparison with a repeat from the low-density lipoprotein receptor. *Biochemistry 37*:17016–17023.

Doreleijers J, Rullmann J, Kaptein R. 1998. Quality assessment of NMR structures: A statistical survey. *J Mol Biol 281*:149–164.

Downing AK, Knott V, Werner JM, Cardy CM, Campbell ID. 1996. Solution structure of a pair of calcium-binding epidermal growth factor-like domains: Implications for the marfan syndrome and other genetic disorders. *Cell 85*:597–605.

Esser V, Limbird LE, Brown MS, Goldstein JL, Russell DW. 1988. Mutational analysis of the ligand binding domain of the low density lipoprotein receptor. *J Biol Chem 263*:13282–13290.

Evans JNS. 1995. *Biomolecular NMR spectroscopy*. New York: Oxford University Press.

Fass D, Blacklow S, Kim PS, Berger JM. 1997. Molecular basis of familial hypercholesterolaemia from structure of LDL receptor module. *Nature 388*:691–693.

Goldstein JL, Brown MS, Anderson RG, Russell DW, Schneider WJ. 1985. Receptor-mediated endocytosis: Concepts emerging from the LDL receptor system. *Annu Rev Cell Biol 1*:1–39.

Griesinger C, Sørenson OW, Ernst RR. 1987. Practical aspects of the E.COSY technique, measurement of scalar spin-spin coupling constants in peptides. *J Magn Reson 75*:474–492.

Güntert P, Mumenthaler C, Wüthrich K. 1997. Torsion angle dynamics for NMR structure calculation with the new program DYANA. *J Mol Biol 273*:283–298.

Havel RJ, Kane JP. 1995. Introduction: Structure and metabolism of plasma lipoproteins. In: Scriver CR, Beaudet AL, Sly WS, Valle D, eds. *The metabolic and molecular basis of inherited disease*. New York: McGraw-Hill. pp 1841–1851.

Herz J, Hamann U, Rogne S, Myklebost O, Gausepohl H, Stanley KK. 1988. Surface location and high affinity for calcium of a 500-kd liver membrane protein closely related to the LDL-receptor suggest a physiological role as lipoprotein receptor. *EMBO J 7*:4119–4127.

Huang W, Dolmer K, Gettins PGW. 1999. NMR solution structure of complement-like repeat CR8 from the low density lipoprotein receptor-related protein. *J Biol Chem 274*:14130–14136.

Jeener J, Meier BH, Bachmann P, Ernst RR. 1979. Investigation of exchange process by two-dimensional NMR spectroscopy. *J Chem Phys 71*:4546–4553.

Jensen HK, Jensen LG, Hansen PS, Faergeman O, Gregersen N. 1996. The Trp^{23}-stop and Trp^{66}-Gly mutations in the LDL receptor gene: common causes of familial hypercholesterolemia in Denmark. *Atherosclerosis 120*:57–65.

Johnson WJ, Phillips MC, Rothblat GH. 1997. Lipoproteins and cellular cholesterol homeostasis. In: Bittman R, ed. *Subcellular biochemistry: Choles-*

terol: Its functions and metabolism in biology and medicine, Vol. 28. New York: Plenum Press. pp 235–276.

Kabsch W, Sander C. 1983. Dictionary of protein secondary structure: pattern recognition of hydrogen-bonded and geometrical features. *Biopolymers 22*:2577–2637.

Kay LE, Forman-Kay JD, Cubbin, WD, Kay CM. 1991. Solution structure of a polypeptide dimmer comprising the fourth Ca^{2+} binding site of troponin C by nuclear magnetic resonance spectroscopy. *Biochemistry 30*:4323–4333.

Koradi R, Billeter M, Wüthrich K. 1996. MOLMOL: A program for display and analysis of macromolecular structures. *J Mol Graphics 14*:51–55.

Laskowski RA, Rullman JAC, MacArthur MW, Kaptein R, Thornton JM. 1996. AQUA and PROCHECK-NMR: Programs for checking the quality of protein structures by NMR. *J Biomol NMR 8*:477–486.

Millhauser GL, Stenland CJ, Hanson H, Bolin KA, van de Ven FJM. 1997. Estimating the relative populations of 3_{10}-helix and α-helix in Ala-rich peptides: A hydrogen exchange and high field NMR study. *J Mol Biol 267*: 964–974.

Moorjani S, Roy M, Torres A, Betard C, Gagne C, Lambert M, Brun D, Davignon J, Lupien P. 1993. Mutations of low-density-lipoprotein-receptor gene, variation in plasma cholesterol, and expression of coronary heart disease in homozygous familial hypercholesterolaemia. *Lancet 341*:1303–1306.

Mumenthaler C, Güntert P, Braun W, Wüthrich K. 1997. Automated combined assignment of NOESY spectra and three-dimensional protein structure determination. *J Biomol NMR 10*:351–362.

North CL, Blacklow SC. 1999. Structural independence of ligand-binding modules five and six of the LDL-receptor. *Biochemistry 38*:3926–3935.

Piotto M, Saudek V, Sklenar V. 1992. Gradient-tailored excitation for single-quantum NMR spectroscopy of aqueous solutions. *J Biomol NMR 2*:661–665.

Rance M, Sørenson, OW, Bodenhausen G, Wagner G, Ernst RR, Wüthrich K. 1983. Improved spectra resolution in COSY ^{1}H spectra of proteins via double quantum filtering. *Biochem Biophys Res Commun 117*:479–485.

Rødningen OK, Tonstand S, Medh JD, Chapell DA, Ose L, Leren TP. 1999. Phenotypic consequences of a deletion of exons 2 and 3 of the LDL receptor gene. *J Lipid Res 40*:213–220.

Russell DW, Brown MS, Goldstein JL. 1989. Different combinations of cysteine-rich repeats mediate binding of low density lipoprotein receptor to two different proteins. *J Biol Chem. 264*:21682–21688.

Saito A, Pietromonaco S, Loo AK, Farquhar MG. 1994. Complete cloning and sequencing of rat gp330/"megali," a distinctive member of the low density lipoprotein receptor gene family. *Proc Natl Acad Sci USA 91*:9725–9729.

Sass C, Giroux LM, Lussier CS, Davignon J, Minnich A. 1995. Unexpected consequences of deletion of the first two repeats of the ligand-binding domain from the low density lipoprotein receptor. Evidence from a human mutation. *J Biol Chem 270*:25166–25171.

Simmons T, Newhouse YM, Arnold KS, Innerarity TL, Weisgraber KH. 1997. Human low density lipoprotein receptor fragment. Successful refolding of a functionally active ligand-binding domain produced in *Escherichia coli*. *J Biol Chem 272*:25531–25536.

Sklenar V, Piotto M, Leppick R, Saudek V. 1993. Gradient-tailored water suppression for H1-N15 HSQC experiments optimized to retain full sensitivity. *J Magn Reson Ser A 102*:241–245.

Slupsky CM, Sykes BD. 1995. NMR solution structure of calcium-saturated skeletal muscle troponin C. *Biochemistry 34*:15953–15964.

Smith LJ, Bolin KA, Schwalbe H, MacArthur MW, Thornton JM, Dobson CM. 1996. Analysis of main chain torsion angles in protein: Prediction of NMR coupling constants for native and random coil conformations. *J Mol Biol 255*:494–506.

Takahashi S, Kawarabayasi Y, Nakai T, Sakai J, Yamamoto T. 1992. Rabbit very low density lipoprotein receptor: A low density lipoprotein receptor-like protein with distinct ligand specificity. *Proc Natl Acad Sci USA 89*:9252–9256.

van Driel IR, Goldstein JL, Sudhof TC, Brown MS. 1987. First cysteine-rich repeat in ligand-binding domain of low density lipoprotein receptor binds Ca^{++} and monoclonal antibodies, but not lipoproteins. *J Biol Chem 262*:17443–17449.

Williamson MP, Havel TF, Wüthrich K. 1985. Solution structure of proteinase inhibitor IIA from bull seminal plasma by ^{1}H nuclear magnetic resonance and distance geometry. *J Mol Biol 182*:295–315.

Wilson C, Wardell MR, Weisgraber KH, Mahley RW, Agard DA. 1991. Three-dimensional structure of the LDL receptor-binding domain of human apolipoprotein E. *Science 252*:1817–1822.

Wüthrich K. 1986. *NMR of proteins and nucleic acids*. New York: Wiley-Interscience.